Article

Photoionization of 1-Alkenylperoxy and Alkylperoxy Radicals and a General Rule for the Stability of Their Cations

Giovanni Meloni, Talitha M. Selby, Fabien Goulay, Stephen R. Leone, David L. Osborn, and Craig A. Taatjes

J. Am. Chem. Soc., **2007**, 129 (45), 14019-14025• DOI: 10.1021/ja075130n • Publication Date (Web): 17 October 2007

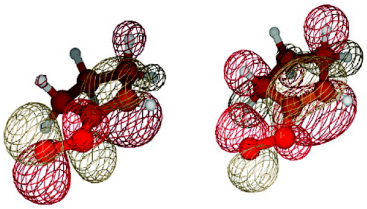

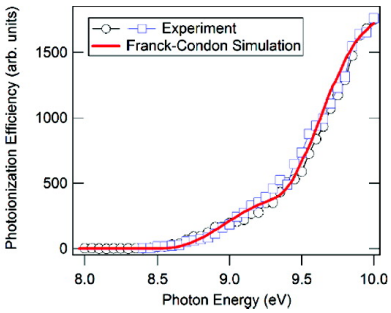

More About This Article

Additional resources and features associated with this article are available within the HTML version:

- Supporting Information
- Links to the 5 articles that cite this article, as of the time of this article download
- Access to high resolution figures
- Links to articles and content related to this article
- Copyright permission to reproduce figures and/or text from this article

View the Full Text HTML

J|A|C|S
ARTICLES
Published on Web 10/17/2007

Photoionization of 1-Alkenylperoxy and Alkylperoxy Radicals and a General Rule for the Stability of Their Cations

Giovanni Meloni,*,† Talitha M. Selby,† Fabien Goulay,‡,§ Stephen R. Leone,‡,§ David L. Osborn,† and Craig A. Taatjes*,†

Contribution from the Combustion Research Facility, Mail Stop 9055, Sandia National Laboratories, Livermore, California 94551-0969, Chemical Sciences Division, Ernest Orlando Lawrence Berkeley National Laboratory, Berkeley, California 94720, and Departments of Chemistry and Physics, University of California, Berkeley, California 94720

Received July 10, 2007; E-mail: gmeloni@sandia.gov; cataatj@sandia.gov

Abstract: The photoionization of 1-alkenylperoxy radicals, which are peroxy radicals where the OO moiety is bonded to an sp^2-hybridized carbon, is studied by experimental and computational methods and compared to the similar alkylperoxy systems. Quantum chemical calculations are presented for the ionization energy and cation stability of several alkenylperoxy radicals. Experimental measurements of 1-cyclopentenylperoxy (1-*c*-C_5H_7OO) and propargylperoxy (CH_2═C═CHOO) photoionization are presented as examples. These radicals are produced by reaction of an excess of O_2 with pulsed-photolytically produced alkenyl radicals. The kinetic behavior of the products confirms the formation of the alkenylperoxy radicals. Electronic structure calculations are employed to give structural parameters and energetics that are used in a Franck−Condon (FC) spectral simulation of the photoionization efficiency (PIE) curves. The calculations also serve to identify the isomeric species probed by the experiment. Adiabatic ionization energies (AIEs) of 1-*c*-C_5H_7OO (8.70 ± 0.05 eV) and CH_2═C═CHOO (9.32 ± 0.05 eV) are derived from fits to the experimental PIE curves. From the fitted FC simulation superimposed on the experimental PIE curves, the splitting between the ground state singlet and excited triplet cation electronic states is also derived for 1-*c*-C_5H_7OO (0.76 ± 0.05 eV) and CH_2═C═CHOO (0.80 ± 0.15 eV). The combination of the AIE(CH_2═C═CHOO) and the propargyl heat of formation provides $\Delta_f H^\circ_0(CH_2{=}C{=}CHOO^+)$ of (1162 ± 8) kJ mol^{-1}. From $\Delta_f H^\circ_0(CH_2{=}C{=}CHOO^+)$ and $\Delta_f H^\circ_0(C_3H_3^+)$ it is also possible to extract the bond energy $D^\circ_0(C_3H_3^+{-}OO)$ of 19 kJ mol^{-1} (0.20 eV). Finally, from consideration of the relevant molecular orbitals, the ionization behavior of alkyl- and alkenylperoxy radicals can be generalized with a simple rule: Alkylperoxy radicals dissociatively ionize, with the exception of methylperoxy, whereas alkenylperoxy radicals have stable singlet ground electronic state cations.

Introduction

Organic peroxy radicals play a pivotal role as reaction intermediates in the low-temperature oxidation and photooxidation of hydrocarbons both in the atmosphere and in combustion processes.[1−3] In particular, alkenylperoxy radicals (R′OO) are intermediates in the oxidation of alkenes, key species in the formation of photochemical smog, a harmful mixture of air pollutants including aldehydes, tropospheric ozone, nitrogen oxides, and volatile organic compounds. Atmospheric alkenes originate from both biogenic and anthropogenic sources. In fact, two-thirds of hydrocarbons emitted into the atmosphere are biogenic unsaturated compounds such as isoprene; thus alkenes represent a substantial portion of the total amount of tropospheric hydrocarbons.[4] Moreover, low-temperature oxidation of alkenes has a considerable impact in the modeling of combustion processes, because of direct combustion of alkenes and because alkenes are intermediates in the combustion of saturated species. Therefore, knowledge of the thermochemistry of R′OO species and the possibility of monitoring them by photoionization are important to several areas of chemistry.

The only previously experimentally studied hydrocarbon peroxy radical cations are CH_3OO^+, $C_2H_5OO^+$, and $C_3H_7OO^+$;[5,6] only the smallest alkylperoxy cation, i.e., CH_3OO^+, shows thermodynamic stability. The triplet ground electronic states of these larger alkylperoxy cations are dissociative because of the relative stability of the alkyl cation fragments with respect to the parent ion arising from hyperconjugative stabilization.

As a part of a continuing effort to characterize the photoionization of noteworthy combustion and atmospheric reaction intermediates, the present work concentrates on 1-alkenylperoxy radicals (i.e., radicals where the OO moiety is bonded to an olefinic carbon). Photoionization efficiency measurements of

† Sandia National Laboratories.
‡ Ernest Orlando Lawrence Berkeley National Laboratory.
§ University of California, Berkeley.

(1) Benson, S. W. *J. Am. Chem. Soc.* **1965**, *87*, 972−979.
(2) Wallington, T. J.; Dagaut, P.; Kurylo, M. J. *Chem. Rev.* **1992**, *92*, 667−710.
(3) Finlayson-Pitts, B. J.; Pitts, J. N. *Science* **1997**, *276*, 1045−52.
(4) Martin, P. H.; Guenther, A. B. *J. Biogeography* **1995**, *22*, 493−499.
(5) Meloni, G.; Zou, P.; Klippenstein, S. J.; Ahmed, M.; Leone, S. R.; Taatjes, C. A.; Osborn, D. L. *J. Am. Chem. Soc.* **2006**, *128*, 13559−13567.
(6) Fu, H. B.; Hu, Y. J.; Bernstein, E. R. *J. Chem. Phys.* **2006**, *125*, 014310.

two 1-alkenylperoxy radicals, 1-cyclopentenylperoxy (1-*c*-C_5H_7-OO), and propargylperoxy (1-propadienylperoxy, $CH_2{=}C{=}CHOO$), are reported, and computational analysis is carried out on several additional representative 1-alkenylperoxy radicals.

1-Propadienyl, $CH_2{=}C{=}\dot{C}H$, is one of two resonant structures of propargyl (the other structure is $\dot{C}H_2{-}C{\equiv}CH$), one of the most important and the simplest resonantly stabilized radicals in combustion.[7] Its resonance stabilization results in low reactivity toward stable species in the combustion environment, enabling relatively large concentrations to be formed in flames. According to Miller and Melius[7] and Miller and Klippenstein,[8] a prominent loss channel for propargyl radicals is self-reaction to produce C_6H_6 species, that depending on the temperature and pressure conditions range from linear 1,5-hexadiyne to the cyclic 3,4-dimethylenecyclobutene, fulvene, benzene, and phenyl + H. These cyclic species are precursors in the production of polycyclic aromatic hydrocarbons, which in turn are precursors of soot.[9,10] An important competing reaction to the "first ring formation" is propargyl oxidation,

$$C_3H_3 + O_2 \rightarrow \text{products} \qquad (1)$$

which, despite its relevance, has been investigated by only a few researchers. Experimental investigations have been carried out by Slagle and Gutman[11] using a sample reactor−mass spectrometric method, by Atkinson and Hudgens,[12] employing laser photolysis coupled with cavity ring-down spectroscopy, and Kong and co-workers,[13] making use of laser photolysis with time-resolved Fourier transform infrared spectroscopy. Kong and co-workers[13] also performed some density functional calculations. Miller and co-workers[14] studied the temperature- and pressure-dependent kinetics with a combination of high-level electronic structure theory, Rice−Ramsperger−Kassel−Marcus (RRKM) theory, and solutions of the time-dependent master equation.

Cyclopentene has recently been the subject of several investigations focused on understanding the initial steps of aromatic ring formation. Fuels containing five-membered carbon rings have anomalously high sooting tendencies, with cyclopentene sooting more readily than other alkenes.[15,16] This experimental observation suggests that C5 rings may play a role in the growth processes that produce aromatic hydrocarbons and, ultimately, soot.[15] Hansen et al.[17,18] carried out experiments with a flame-sampling molecular beam photoionization mass spectrometer employing tunable vacuum-ultraviolet synchrotron radiation to resolve the isomeric composition of the intermediates in a laminar premixed cyclopentene flame. From Franck−Condon simulations of the photoionization efficiency measurements, together with calculated ionization energies, C5 and C7 ring isomers were resolved suggesting potential new pathways in molecular-weight growth mechanisms. Oxidation of these hydrocarbon radicals will be an important process competing with molecular-weight-growth reactions.

In this investigation, we report an experimental determination of the adiabatic ionization energy of 1-cyclopentenylperoxy and propargylperoxy. These measurements are obtained using a multiplexed time-resolved photoionization mass spectrometer that simultaneously probes the formation and depletion of multiple species during photolytically initiated reactions. The photoionization efficiency (PIE) curves of both 1-*c*-C_5H_7OO and $CH_2{=}C{=}CHOO$ show the presence of two electronic transitions, from the ground state of the neutral to the ground and first excited electronic states of the cation. With the help of electronic structure calculations and Franck−Condon (FC) spectral simulations, we find the ground electronic states of 1-alkenylperoxy cations are stable, closed-shell singlets, whereas alkylperoxy cations larger than CH_3OO have unbound, triplet ground electronic states. Computational analysis of several other representative alkenylperoxy radicals and consideration of the nature of the molecular orbitals (MO) participating in the ionization process lead to a general rule predicting that 1-alkenylperoxy cations should have stable singlet ground states.

Experiment Section

Apparatus. The experiments are performed using a time-resolved mass spectrometer that has been described previously[5] in some detail. Schematically, it consists of a slow-flow reactor,[19] in which reactions are photolytically initiated, coupled to a photoionization mass spectrometer. The photolytic precursors used in this investigation are propargyl bromide (>98%) and H_2O_2 that has been generated by thermal decomposition of a urea−hydrogen peroxide adduct (97%), kept in a 45 °C thermostatted bubbler. Photolysis of propargyl bromide at 248 nm yields propargyl radicals that then react with O_2 to form products including propargylperoxy radicals. The 248 nm photolysis of H_2O_2 produces OH radicals that react with cyclopentene (>96%) to form a number of possible radical products that subsequently react with O_2. These subsequent reactions produce cyclopentenylperoxy radicals by cyclopentenyl + O_2 reactions or possibly indirectly via reactions of hydroxycyclopentyl radicals formed by OH addition to cyclopentene.

The KrF excimer laser (248 nm) photolysis beam propagates down the flow reactor, creating a uniform density of radicals (e.g., propargyl) along the length of the tube. The reacting mixture effuses from a pinhole located in the side of the reactor, passes through a skimmer, and enters the ionization region of a miniature double-focusing magnetic-sector mass spectrometer of the Mattauch−Herzog geometry,[20] where the gas beam is crossed by tunable synchrotron undulator radiation that has been dispersed by a 3 m monochromator at the Chemical Dynamics Beamline of the Advanced Light Source at Lawrence Berkeley National Laboratory.

Ions are accelerated, focused, and dispersed according to the square root of their mass in a 0.94 T magnetic field. At the exit plane of the magnet, all ions within a variable mass range of 6× (e.g., $m/z = 14$ to $m/z = 84$) hit the active area of a time- and position-sensitive microchannel plate detector with a delay-line anode.[21] The position and time of arrival with respect to the photodissociation laser are recorded for each ion. The experiment is repeated for up to 20 000 laser pulses to signal average the data.

(7) Miller, J. A.; Melius, C. F. *Combust. Flame* **1992**, *91*, 21−39.
(8) Miller, J. A.; Klippenstein, S. J. *J. Phys. Chem. A* **2003**, *107*, 7783−7799.
(9) Miller, J. A. *Proc. Combust. Inst.* **1996**, *26*, 461−480.
(10) Frenklach, M. *Phys. Chem. Chem. Phys.* **2002**, *4*, 2028−37.
(11) Slagle, I. R.; Ratajczak, E.; Gutman, D. *J. Phys. Chem.* **1986**, *90*, 402−407.
(12) Atkinson, D. B.; Hudgens, J. W. *J. Phys. Chem. A* **1999**, *103*, 4242−4252.
(13) Dong, F.; Wang, S. F.; Kong, F. A. *J. Phys. Chem. A* **2003**, *107*, 9374−9379.
(14) Hahn, D. K.; Klippenstein, S. J.; Miller, J. A. *Faraday Discuss.* **2001**, *119*, 79−100.
(15) McEnally, C. S.; Pfefferle, L. D. *Combust. Sci. Technol.* **1998**, *131*, 323−344.
(16) Gomez, A.; Sidebotham, G.; Glassman, I. *Combust. Flame* **1984**, *58*, 45−57.
(17) Hansen, N.; Klippenstein, S. J.; Miller, J. A.; Wang, J.; Cool, T. A.; Law, M. E.; Westmoreland, P. R.; Kasper, T.; Kohse-Höinghaus, K. *J. Phys. Chem. A* **2006**, *110*, 4376−4388.
(18) Hansen, N.; Kasper, T.; Klippenstein, S. J.; Westmoreland, P. R.; Law, M. E.; Taatjes, C. A.; Kohse-Höinghaus, K.; Wang, J.; Cool, T. A. *J. Phys. Chem. A* **2007**, *111*, 4081 -4092.
(19) Slagle, I. R.; Gutman, D. *J. Am. Chem. Soc.* **1985**, *107*, 5342−5347.
(20) Sinha, M. P.; Wadsworth, M. *Rev. Sci. Instrum.* **2005**, *76*, 025103−8.

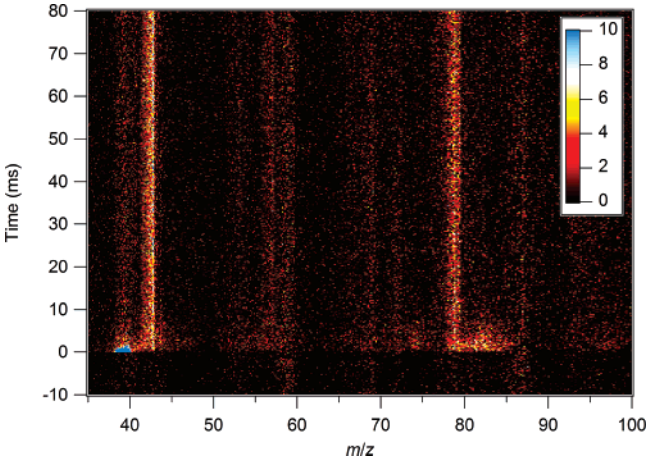

Figure 1. A section of the time-resolved mass spectrum for the reaction of C_3H_3 with O_2 ($[O_2] = 4.7 \times 10^{16}$ molecule cm^{-3}) integrated over photon energies from 9.35 to 10 eV.

The photon energy of the synchrotron can be scanned during an acquisition yielding a complete series of time-resolved mass spectra at each photoionization energy. The photon energy ($h\nu_{ALS}$) and the energy resolution (30 meV for 200 μm exit slit width, 50 meV for 600 μm slit width) are calibrated by measurement of known atomic resonances of Xe and narrow autoionization resonances in O_2. Further confirmation of the energy calibration is made by measurement of the ionization threshold of acetone.[22]

For each experiment the intensity of all the species is recorded as a function of the mass-to-charge ratio, reaction time, and photon energy. An example of a time-resolved mass spectrum is shown for the reaction of C_3H_3 with O_2 taken at a photon energy of 10 eV in Figure 1.

The experimental PIE curve is obtained by integrating such data first over the desired mass-to-charge ratio and then over a time window that corresponds to the production of the species of interest in the photolytically initiated reaction. Background subtraction is performed at the same mass-to-charge ratio by a similarly integrated signal taken before the photolysis laser is pulsed. Finally, this background-subtracted signal at each photon energy is normalized for the ALS photon current and accumulated into the PIE spectrum.

Electronic Structure Calculations. Structural parameters, including bond lengths, harmonic vibrational frequencies, and force constants of the 1-*c*-C_5H_7OO/1-*c*-$C_5H_7OO^+$ and CH_2═C═CHOO/CH_2═C═CHOO$^+$ species are optimized at the Becke three-parameter exchange functional with the Lee, Yang, and Parr correlation functional (B3LYP) method and all electron 6-311+G** basis set, using the Gaussian03 suite.[23] The normal-mode frequencies and force constants are then employed in the Franck−Condon spectral simulation to reproduce the overall shape and onset of the PIE curves. The experimental spectra are identified partly on the basis of their agreement with theoretical ionization energies and Franck−Condon envelopes. The composite CBS-QB3 (complete basis set) model of Petersson and co-workers that combines the general design of the CBS-Q[24,25] energy calculation with the B3LYP/6-311G(d,p) density functional optimized geometries and frequencies[26,27] is employed to supply reliable energetics. This method provides thermochemical values with a mean absolute deviation from experiment of 4−5 kJ mol^{-1} for a reference set of molecules.[27] The results of the energetics are summarized in Table 1, and the optimized molecular parameters are reported in Table 2.

Table 1. CBS-QB3 Energies of the CH_2═C═CHOO/CH_2═C═CHOO$^+$ and 1-*c*-C_5H_7OO/1-*c*-$C_5H_7OO^+$ Systems Together with Other 1-Alkenylperoxy Radicals[a]

species	state	energy	$\langle S^2\rangle$	$H^\circ_{298} - H^\circ_0$	D_0(R′–OO)
$OOCH_2$—C≡CH[b]	$\tilde{X}\,^2A''$	0.07	0.753	17.2	-
CH_2═C═CHOO	$\tilde{X}\,^2A''$	0	0.756	16.8	0.86
CH_2═C═CHOO$^+$	$\tilde{X}\,^1A'$	9.36	-	16.3	0.24
CH_2═C═CHOO$^+$	$\tilde{a}\,^3A''$	10.04	2.010	17.4	-
1-*c*-C_5H_7OO	$\tilde{X}\,^2A$	0	0.760	19.6	2.17
1-*c*-$C_5H_7OO^+$	$\tilde{X}\,^1A$	8.71	-	19.9	1.26
1-*c*-$C_5H_7OO^+$	$\tilde{a}\,^3A$	9.40	2.006	20.4	-
CH_2═CHOO	$\tilde{X}\,^2A''$	0	0.757	14.0	1.94
CH_2═CHOO$^+$	$\tilde{X}\,^1A'$	9.81	-	13.4	0.65
CH_2═CHOO$^+$	$\tilde{a}\,^3A''$	10.34	2.016	14.2	-
$CH_3C(OO)$═CH_2	$\tilde{X}\,^2A''$	0	0.760	17.1	1.96
$CH_3C(OO)$═CH_2^+	$\tilde{X}\,^1A'$	9.32	-	16.9	0.26
$CH_3C(OO)$═CH_2^+	$\tilde{a}\,^3A''$	9.93	2.017	18.2	-
1-*c*-C_6H_9OO	$\tilde{X}\,^2A$	0	0.760	22.1	2.07
1-*c*-$C_6H_9OO^+$	$\tilde{X}\,^1A$	8.58	-	21.9	0.80
1-*c*-$C_6H_9OO^+$	$\tilde{a}\,^3A$	9.40	2.001	22.8	-
C_6H_5OO	$\tilde{X}\,^2A''$	0	0.750	19.1	2.31
$C_6H_5OO^+$	$\tilde{X}\,^1A'$	8.95	-	19.0	1.54
$C_6H_5OO^+$	$\tilde{a}\,^3A''$	9.69	2.000	19.5	-

[a] All energies, in eV, are corrected for the zero-point vibrational energy and are relative to the neutral ground electronic state. The heat content functions ($H^\circ_{298} - H^\circ_0$) are in kJ mol^{-1}. [b] From the CBS-QB3 calculations this peroxy isomer dissociatively ionizes at 9.47 eV to $C_3H_3^+ + O_2$.

Table 2. Bond Distances (Å) and Angles (deg) Optimized at the B3LYP/6-311+G** Level of Theory

molecule	$r_{C_\alpha=C_\beta}$	$r_{C_\alpha-O}$	r_{O-O}	$\angle C_\alpha OO$	θ[a]
$\tilde{X}\,^2A''$ CH_2═C═CHOO	1.31	1.40	1.32	112	180
$\tilde{X}\,^1A'$ CH_2═C═CHOO$^+$	1.35	1.34	1.25	118	180
$\tilde{a}\,^3A''$ CH_2═C═CHOO$^+$	1.32	1.39	1.28	121	180
$\tilde{X}\,^2A$ 1-*c*-C_5H_7OO	1.34	1.37	1.33	114	177
$\tilde{X}\,^1A$ 1-*c*-$C_5H_7OO^+$	1.39	1.32	1.28	117	179
$\tilde{a}\,^3A$ 1-*c*-$C_5H_7OO^+$	1.40	1.34	1.35	114	174
$\tilde{X}\,^2A''$ CH_2═CHOO	1.33	1.38	1.32	113	180
$\tilde{X}\,^1A'$ CH_2═CHOO$^+$	1.36	1.35	1.24	119	180
$\tilde{a}\,^3A''$ CH_2═CHOO$^+$	1.35	1.37	1.28	122	180
$\tilde{X}\,^2A''$ $CH_3C(OO)$═CH_2	1.33	1.39	1.32	115	180
$\tilde{X}\,^1A'$ $CH_3C(OO)$═CH_2^+	1.37	1.37	1.25	118	180
$\tilde{a}\,^3A''$ $CH_3C(OO)$═CH_2^+	1.37	1.36	1.30	121	180
$\tilde{X}\,^2A$ 1-*c*-C_6H_9OO	1.33	1.39	1.32	115	178
$\tilde{X}\,^1A$ 1-*c*-$C_6H_9OO^+$	1.39	1.33	1.27	118	178
$\tilde{a}\,^3A$ 1-*c*-$C_6H_9OO^+$	1.39	1.35	1.33	118	171
$\tilde{X}\,^2A''$ C_6H_5OO	1.39	1.40	1.32	116	180
$\tilde{X}\,^1A'$ $C_6H_5OO^+$	1.42	1.33	1.26	121	180
$\tilde{a}\,^3A''$ $C_6H_5OO^+$	1.42	1.35	1.31	121	180

[a] θ is the dihedral angle formed by the C_β═C_α—O—O bonds.

For all states presented in Table 1, the spin expectation value, $\langle S^2\rangle$ is evaluated to check for possible spin-contaminated wave functions,[28] which is negligible in all cases. All frequencies are found to be real, indicating that our geometries represent minima on the potential energy surface. In both alkenylperoxy species the O_2 group is in the anti position with respect to the double bond. For C_3H_3OO, two different peroxy radicals, $OOCH_2$—C≡CH and CH_2═C═CHOO, are possible, derived from O_2 addition to the two resonance structures of propargyl. The 1-alkenylperoxy, CH_2═C═CHOO, is 0.07 eV (7 kJ mol^{-1}) more stable than $OOCH_2$—C≡CH.

To strengthen our generalization on the photoionization behavior of alkenyl-type peroxy radicals, CBS-QB3 calculations on vinylperoxy

(21) Vallerga, J. V.; Siegmund, O. H. W. *Nucl. Inst. Methods Phys. Res. A* **2000**, *442*, 159−163.
(22) Trott, W. M.; Blais, N. C.; Walters, E. A. *J. Chem. Phys.* **1978**, *69*, 3150−3158.
(23) Frisch, M. J., et al. *Gaussian 03*, revision C.02; Gaussian, Inc.: Wallingford, CT, 2004.
(24) Ochterski, J. W.; Petersson, G. A.; Montgomery, J. A. *J. Chem. Phys.* **1996**, *104*, 2598−2619.
(25) Montgomery, J. A., Jr.; Frisch, M. J.; Ochterski, J. W.; Petersson, G. A.; Raghavachari, K.; Zakrzewski, V. G. *J. Chem. Phys.* **1998**, *109*, 6505−6.
(26) Montgomery, J. A.; Frisch, M. J.; Ochterski, J. W.; Petersson, G. A. *J. Chem. Phys.* **1999**, *110*, 2822−7.
(27) Montgomery, J. A.; Frisch, M. J.; Ochterski, J. W.; Petersson, G. A. *J. Chem. Phys.* **2000**, *112*, 6532−42.
(28) Mayer, P. M.; Parkinson, C. J.; Smith, D. M.; Radom, L. *J. Chem. Phys.* **1998**, *108*, 604−15.

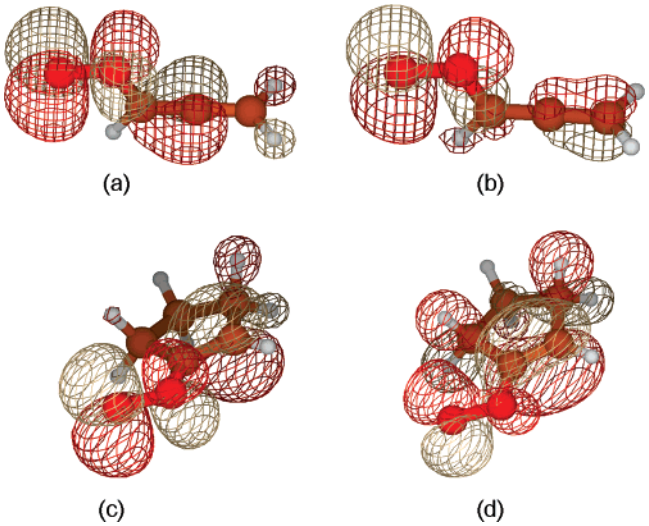

Figure 2. Outer molecular orbitals for CH_2═C═CHOO [(a) HOMO and (b) HOMO−1] and 1-*c*-C_5H_7OO [(c) HOMO and (d) HOMO−1].

(CH_2═CHOO), 2-propenylperoxy ($CH_3CH(OO)$═CH_2), 1-cyclohexenylperoxy (1-*c*-C_6H_9OO), and phenylperoxy (C_6H_5OO) have been performed as well. The results are listed in Tables 1 and 2. All these species are predicted to have cations with a bound singlet ground electronic state.

Results and Discussion

Upon ionization of the neutral 1-*c*-C_5H_7OO and CH_2═C═CHOO radicals, the formation of the ground and first excited electronic states are accompanied by geometry changes (see Table 2) that can be explained in terms of a simplified molecular orbital picture. In this regard, the MOs of the neutral species can be thought of as a linear combination of the molecular orbitals of the two dissociation fragments, R′ (1-*c*-C_5H_7 and C_3H_3) and O_2. In particular, the highest occupied molecular orbital (HOMO) of both of the neutral species can be seen as a $\pi^*_{C_\alpha-O}$ MO, originating from the combination of the bonding $\pi_{C_\alpha=C_\beta}$ MO of R′ and the antibonding O_2 π^* MO, whereas the HOMO-1 is different for the two molecules. For CH_2═C═CHOO the HOMO-1 can be visualized as a nonbonding C_α—O MO, composed from the combination of a bonding $\sigma_{C_\alpha-H}$ orbital and the antibonding O_2 π^* MO. For 1-*c*-C_5H_7OO the HOMO-1 can be thought of as a partially antibonding $\pi^*_{C_\alpha-O}$ MO, from the combination of the bonding $\pi_{C_\alpha=C_\beta}$ and the antibonding O_2 π^* MO, but with more electronic density in the C5 ring than in the HOMO. For clarification of the following arguments, the HOMO and HOMO-1 of propargylperoxy and 1-cyclopentenylperoxy are shown in Figure 2. From these MO combinations it is straightforward to rationalize the bond length changes upon removal of an electron from the HOMO of the neutral to generate the cation ground electronic state and from the HOMO−1 to generate the cation first excited electronic state. The character of the relevant MOs can be qualitatively seen in the bond distance changes upon photoionization. For the $\tilde{X}$ (cation) + e^- ← $\tilde{X}$ (neutral) transition, we have a shortening of the O_2 bond distance, lengthening of $r_{C_\alpha=C_\beta}$, and decrease of the $r_{C_\alpha-O}$ length. The decrease in the C_α—O bond length ($\Delta r_{C_\alpha-O}$ = −0.05 Å between CH_2═C═CHOO and CH_2═C═$CHOO^+$, and $\Delta r_{C_\alpha-O}$ = −0.06 Å between 1-*c*-C_5H_7-OO and 1-*c*-$C_5H_7OO^+$) can be associated with the removal of an electron from an MO with an antibonding $\pi^*_{C_\alpha-O}$ character

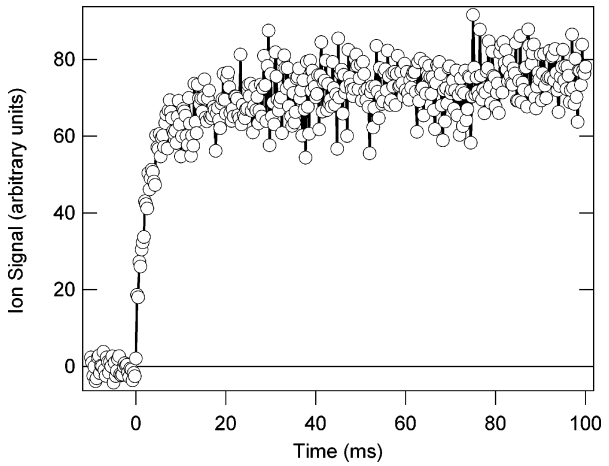

Figure 3. Time profile of 1-*c*-C_5H_7OO obtained by integrating the ion signal over photon energies from 8.5 to 10 eV.

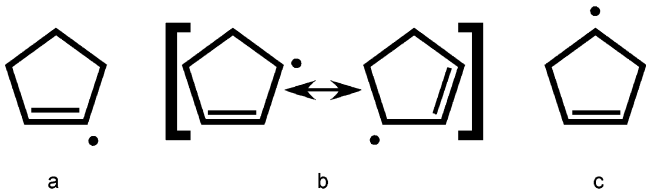

Figure 4. Cyclopentenyl radicals: (a) 1-*c*-C_5H_7 ("vinylic radical"), (b) 2-*c*-C_5H_7 ("allylic radical"), and (c) 3-*c*-C_5H_7 ("alkylic radical").

(decrease of the bond length caused by an increased bond order). An increase in the carbon−carbon double length ($\Delta r_{C_\alpha=C_\beta}$ = +0.04 Å between CH_2═C═CHOO and CH_2═C═$CHOO^+$, and $\Delta r_{C_\alpha=C_\beta}$= +0.05 Å between 1-*c*-$C_5H_7OO$ and 1-*c*-$C_5H_7OO^+$) can be rationalized by the removal of an electron from an MO with a bonding $\pi_{C_\alpha=C_\beta}$ character (increase of the bond length caused by a decreased bond order). In addition, the r_{O-O} decrease results from removal of an electron from the antibonding O_2 π^* MO. For the $\tilde{a}^3A$ (cation) + e^- ← $\tilde{X}$ (neutral) transition, $r_{C_\alpha=C_\beta}$ and $r_{C_\alpha-O}$ are almost identical for both $\tilde{X}$ ^2A CH_2═C═CHOO and $\tilde{a}^3A$ CH_2═C═$CHOO^+$ states owing to the fact that the HOMO−1 of the neutral has negligible $C_\alpha C_\beta$ MO character and is nonbonding with respect to C_α—O. By contrast, $r_{C_\alpha=C_\beta}$ increases (by 0.06 Å) and $r_{C_\alpha-O}$ decreases (by 0.03 Å) between $\tilde{X}$ ^2A 1-*c*-C_5H_7OO and $\tilde{a}^3A$ 1-*c*-$C_5H_7OO^+$, reflecting both the bonding $\pi_{C_\alpha=C_\beta}$ and partially antibonding $\pi^*_{C_\alpha-O}$ nature of the HOMO−1 in that molecule. The O—O bond distance decreases between $\tilde{X}$ ^2A CH_2═C═CHOO and $\tilde{a}^3A$ CH_2═C═$CHOO^+$ because of the O_2 π^* character, whereas it slightly increases between $\tilde{X}$ ^2A 1-*c*-C_5H_7OO and $\tilde{a}^3A$ 1-*c*-C_5H_7-OO^+.

1-*c*-C_5H_7OO. As stated in the Experimental Section, the formation of the cyclopentenylperoxy radical is initiated by reaction of OH with cyclopentene. Because of the time-resolution capability of the apparatus, the temporal ion signal profile of 1-*c*-$C_5H_7OO^+$ is monitored. The signal shows the same time dependence at each photon energy and exhibits the typical time profile for a reaction product, as shown in Figure 3. The removal of the peroxy radicals in this system proceeds by relatively slow radical−radical reactions, so the signal persists to long reaction times. The OH radical can abstract a hydrogen atom from three different sites of cyclopentene, making three possible cyclopentenyl radicals (see Figure 4), i.e., 1-*c*-C_5H_7 ("vinylic radical"), 2-*c*-C_5H_7 ("allylic radical"), and 3-*c*-C_5H_7

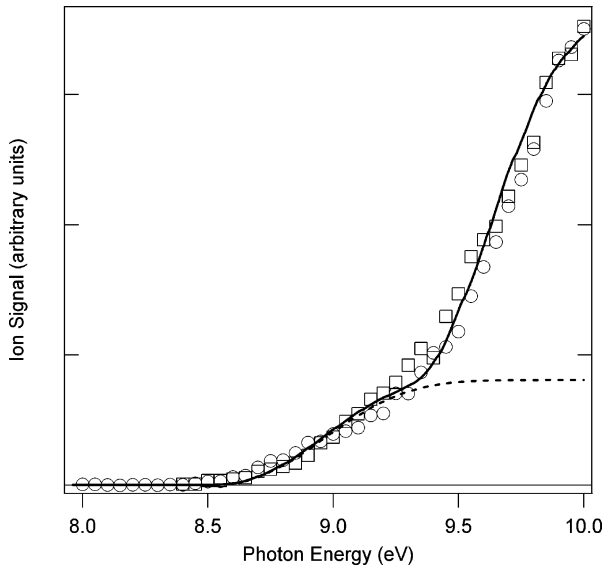

Figure 5. The calculated Franck−Condon PIE curve (thick solid line) for 1-*c*-C_5H_7OO is superimposed on the experimental PIE curves (open symbols − circles and squares taken from two separate determinations), measured with a 0.050 eV step size and an ∼0.05 eV (fwhm) energy resolution. The dashed line represents the calculated FC PIE curve considering only the ground-state-to-ground-state transition.

("alkylic radical"). (Conceivably, the peroxy radicals could also be formed by more complex chemistry subsequent to OH addition to cyclopentene, but that would not affect the spectroscopic work described here.) According to the CBS-QB3 calculations, the most stable cyclopentenyl radical is 2-*c*-C_5H_7, which is resonantly stabilized, followed by the 3-*c*-C_5H_7 (55 kJ mol^{-1} higher in energy) and 1-*c*-C_5H_7 (126 kJ mol^{-1} higher in energy). These energy differences are noticeably reduced in the associated peroxy radicals, with the 2-*c*-C_5H_7OO the most stable, followed by 1-*c*-C_5H_7OO (2.3 kJ mol^{-1} higher) and 3-*c*-C_5H_7OO (4.5 kJ mol^{-1} higher). From this representation, it may seem that the observed PIE curve should be a combination of the photoionization of the three peroxy radicals. In fact, the CBS-QB3 calculations reveal that only the 1-*c*-C_5H_7OO isomer has a cation with a ground electronic state bound by 1.26 eV with respect to the ground electronic state dissociation products, 1-*c*-$C_5H_7^+ + O_2$. The other two radicals have unbound or very weakly bound cations, implying that only one isomer should appear in the PIE spectrum at the parent mass. Specifically, the ground states of 2-*c*-$C_5H_7OO^+$ and 3-*c*-$C_5H_7OO^+$ are only weakly bound, by 0.08 and 0.10 eV, with respect to the ground state dissociation products, 2-*c*-$C_5H_7^+ + O_2$ and 3-*c*-$C_5H_7^+ + O_2$, and they resemble the optimized dissociation products with very long R′ −OO distances of 3.26 Å for 2-*c*-$C_5H_7OO^+$ and 2.85 Å for 3-*c*-$C_5H_7OO^+$.

The photoionization efficiency curve of 1-cyclopentenylperoxy, presented in Figure 5, exhibits an onset at around 8.7 eV and a second feature at ∼9.5 eV with a steeper threshold. No vibrationally resolved structure is observed. The analysis of this data is aided by a Franck−Condon (FC) simulation of the PIE curve, using the optimized geometries and force constants for both the neutral and cation electronic states obtained from the B3LYP/6-311+G** level of theory. The spectral simulation of the PIE curve is carried out by computation and integration of the photoelectron spectrum of 1-*c*-C_5H_7OO, within the FC approximation and including Duschinsky rotation,[29] using the PESCAL program.[30,31] The resulting simulation of the data is convolved with the measured experimental energy resolution, and the fit is optimized by varying the ionization energies of the two cation electronic states and the ratio of their ionization cross sections, as in previous work.[5,32] For comparison, the best fit PIE curve at a temperature of 300 K is superimposed on the experimental curve shown in Figure 5, supporting the identification as 1-*c*-C_5H_7OO. Contributions from the 2-*c*-C_5H_7OO isomer are ruled out because the calculated ionization energy (7.83 eV) is far below the observed threshold, and ionization of the 3-*c*-C_5H_7OO isomer (with a predicted ionization energy of 8.74 eV) would exhibit a much more extended (over several eV) Franck−Condon progression.

The two features observed in the experimental PIE curve can be assigned to the $\tilde{X}\ ^1A + e^- \leftarrow \tilde{X}\ ^2A$ and $\tilde{a}^3A + e^- \leftarrow \tilde{X}\ ^2A$ transitions based on the CBS-QB3 calculations. The transition from the ground electronic state of the neutral to the ground electronic state of the cation provides the adiabatic ionization energy (AIE), and the transition to the first excited state of the cation provides indirectly the term energy of the triplet state of 1-*c*-$C_5H_7OO^+$. For the ground-state-to-ground-state transition, the five most active vibrational modes are utilized in the FC simulation. The modes that show the largest displacement upon photoionization are ν_1 and ν_3, corresponding, respectively, to the torsion of the terminal oxygen and the rocking motion of O−O with respect to R′. For the ground state to first excited-state transition four active modes are included. Also in this case, the mode that displays the largest displacement is ν_1.

It is common practice to estimate the AIE from the midpoint rise of a vibrational threshold in a photoionization efficiency spectrum. In the case of 1-*c*-C_5H_7OO, no vibrationally resolved threshold is observed, and the present determination for the AIE of 8.70 ± 0.05 eV is based on a fit of the experimental PIE curve to a sum of the Franck−Condon envelopes for ionization to the singlet and triplet states. This best fit is obtained by fixing the integrated cross sections for ionization to the singlet and triplet cation electronic states as $\sigma(\tilde{X})/\sigma(\tilde{a}) = 0.22$. The total uncertainty derives from many considerations, such as the approximate nature of calculated Franck−Condon factors, the photon energy calibration, possible presence of hot bands, and field ionization of high-lying Rydberg states. The splitting between the singlet and triplet cation states is calculated to be 0.69 eV with the CBS-QB3 method, and this value has been varied to best reproduce the overall experimental PIE curve shape, yielding a fitted value of (0.76 ± 0.05) eV. The CBS-QB3 AIE for 1-*c*-C_5H_7OO, 8.71 eV, is in very close agreement with the experimental result. To check against possible contamination of the peroxy signal from molecules heavier by one mass unit, calculations on the hydroperoxides, 1-*c*-C_5H_7OOH, 2-*c*-C_5H_7OOH, and 3-*c*-C_5H_7OOH have also been performed with the CBS-QB3 method. The computational results show that these hydroperoxides have much different ionization energies than 1-*c*-C_5H_7OO, specifically AIE(1-*c*-C_5H_7OOH) = 8.16 eV, AIE(2-*c*-C_5H_7OOH) = 9.08 eV, and AIE(3-*c*-C_5H_7OOH) = 9.33 eV.

(29) Duschinsky, F. *Acta Physicochim. URSS* **1937**, *7*, 551.
(30) Ervin, K. M.; Ramond, T. M.; Davico, G. E.; Schwartz, R. L.; Casey, S. M.; Lineberger, W. C. *J. Phys. Chem. A* **2001**, *105*, 10822−10831.
(31) Ervin, K. M. *PESCAL*, Fortran program, 2004.
(32) Taatjes, C. A.; Osborn, D. L.; Cool, T. A.; Nakajima, K. *Chem. Phys. Lett.* **2004**, *394*, 19−24.

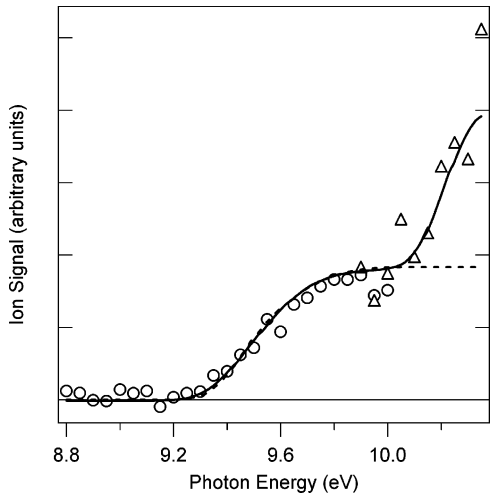

Figure 6. The Franck−Condon calculated PIE curve (thick solid line) for CH_2═C═CHOO is superimposed on the experimental PIE curve (open symbols), taken with a 0.050 eV step size and an ~0.05 eV (fwhm) energy resolution. The dashed line represents the calculated FC PIE curve considering only the ground-state-to-ground-state transition.

Because of large signal from cyclopentene at the adjacent mass, no dissociative ionization of 1-*c*-C_5H_7OO to cyclopentenyl cation and O_2 could be observed, and the 1-*c*-C_5H_7−OO bond energy could not be measured experimentally. Nevertheless, the CBS-QB3 computed bond energy of 2.17 eV indicates a strong bonding interaction between 1-*c*-C_5H_7 and O_2. This result is not unexpected for "vinylic C"−O_2 bonds, for which the D_0°(R′−OO) values are relatively high, such as in vinylperoxy, where $D_0^\circ(C_2H_3-OO) = 1.79$ eV (obtained from the enthalpies of formation at 298.15 K of C_2H_3 [33] and C_2H_3OO[34] corrected to 0 K), and in phenylperoxy, where $D_0^\circ(C_6H_5-OO)$ is between 1.86 eV and 2.01 eV.[35,36]

CH_2═C═CHOO. Propargyl, obtained from the 248 nm photolysis of propargyl bromide, is a resonantly stabilized radical, possessing two resonance structures: $\dot{C}H_2$−C≡CH and CH_2═C═$\dot{C}$H, the first of which is dominant. In the reaction with propargyl, O_2 can add to either radical site. From the CBS-QB3 calculations, the peroxy radical bonded to the sp^2 C, i.e., 1-propadienylperoxy, has a bound cation by 0.24 eV with respect to the ground electronic state dissociation products, $C_3H_3^+ + O_2$, implying that only one isomer should be present in the PIE spectrum. The other "alkylic-type" propargylperoxy cation is only weakly bound by 0.07 eV with respect to the ground state dissociation products and shows a long R′−OO distance of 2.48 Å yielding a very extended Franck−Condon envelope for ionization.

The CH_2═C═$CHOO^+$ PIE curve, shown in Figure 6, presents two features at ~9.3 and 10 eV, with no evident vibrational thresholds. In the FC simulation, five active vibrational frequencies have been used for the $\tilde{X}\ ^1A + e^- \leftarrow \tilde{X}\ ^2A$ transition, and four active frequencies, for the $\tilde{a}^3A + e^- \leftarrow \tilde{X}\ ^2A$ transition. For the ground-state-to-ground-state and ground-state-to-first-excited-state transitions the most active modes are the C−C−C and the O_2 in-plane bending modes. The time trace of CH_2═C═$CHOO^+$ displays relatively poor signal-to-noise but shows production on a millisecond time scale, consistent with formation from propargyl + O_2.[11,37] The propargylperoxy peaks in the first 5 to 10 ms after the photolysis laser and settles to a steady level.

From the calculated energies and the best fit to the FC simulation, the onsets can be assigned to the $\tilde{X}\ ^1A + e^- \leftarrow \tilde{X}\ ^2A$ and (tentatively) $\tilde{a}^3A + e^- \leftarrow \tilde{X}\ ^2A$ electronic transitions. The fit yields an experimental AIE of (9.32 ± 0.05) eV, in close agreement with the CBS-QB3 value of 9.36 eV, and a splitting between the cation triplet and singlet states of (0.8 ± 0.15) eV, compared to the CBS-QB3 prediction of 0.69 eV. This best fit is obtained by fixing the ionization cross sections of the singlet and triplet electronic states as $\sigma(\tilde{X})/\sigma(\tilde{a}) = 0.46$. The uncertainty in the experimental cation state energy is increased because of lower signal-to-noise, particularly for the triplet cation state, whose detection as a result is somewhat uncertain. Observation of the triplet state is surprising, as it is predicted to be thermodynamically unbound (see Table 1), unlike the lowest triplet of 1-*c*-$C_5H_7OO^+$. However, the calculated geometry of the triplet CH_2═C═$CHOO^+$ is very much like the stable cations, with a small C−O bond length (Table 2). Production of parent cations would imply a substantial barrier to dissociation on the triplet surface. It is also possible that the increase in signal at higher photon energy arises from dissociative ionization of an undetermined higher-mass product.

Slagle and Gutman[11] in a kinetics experiment measured the propargyl−OO bond energy at 298 K as (79 ± 6) kJ mol^{-1} or (74 ± 6) kJ mol^{-1} after correction to 0 K using the heat capacity functions. This bond energy corresponds to the "alkyl-type" propargylperoxy formed by adding O_2 to the terminal CH_2 of the dominant resonance structure, i.e., $OOCH_2$−C≡CH. In fact, according to the theoretical analysis by Hahn et al.,[14] formation of 1-propadienylperoxy, CH_2═C═CHOO, proceeds over an ~12 kJ mol^{-1} barrier, whereas addition to the other radical site is almost barrierless. This is one reason why the 1-propadienylperoxy signal is low (Figure 1). From the CBS-QB3 energetics the bond energy at 0 K for CH_2CCH−OO can be estimated as (81 ± 6) kJ mol^{-1} by adding the energy difference between the two propargylperoxy isomers to the experimental D_0°(OO−CH_2CCH) of Slagle and Gutman. This value is reproduced very well by the direct computation of the bond energy of CH_2═C═CHOO, $D_0^\circ(CH_2CCH-OO) = 0.86$ eV (83 kJ mol^{-1}).

From a semiempirical $D_0^\circ(CH_2CCH-OO)$ of (81 ± 6) kJ mol^{-1} and an enthalpy of formation at 0 K for propargyl of (344 ± 4) kJ mol^{-1} (after correction to 0 K using the corresponding heat capacity functions) from King and Nguyen,[38] we obtain $\Delta_f H_0^\circ(CH_2$═C═CHOO) of (263 ± 7) kJ mol^{-1} using the relationship

$$\Delta_f H_0^\circ(CH_2\text{═}C\text{═}CHOO) = \Delta_f H_0^\circ(C_3H_3) - D_0^\circ(CH_2CCH-OO) \quad (2)$$

This value is in excellent agreement with the directly calculated CBS-QB3 $\Delta_f H_0^\circ(CH_2$═C═CHOO) value of 261 kJ mol^{-1}. The experimental determination of AIE(CH_2═C═CHOO) together

(33) Ervin, K. M.; Gronert, S.; Barlow, S. E.; Gilles, M. K.; Harrison, A. G.; Bierbaum, V. M.; DePuy, C. H.; Lineberger, W. C.; Ellison, G. B. *J. Am. Chem. Soc.* **1990**, *112*, 5750−5759.
(34) Fahr, A.; Hassanzadeh, P.; Laszlo, B.; Huie, R. E. *Chem. Phys.* **1997**, *215*, 59−66.
(35) Mebel, A. M.; Lin, M. C. *J. Am. Chem. Soc.* **1994**, *116*, 9577−9584.
(36) Tokmakov, I. V.; Kim, G. S.; Kislov, V. V.; Mebel, A. M.; Lin, M. C. *J. Phys. Chem. A* **2005**, *109*, 6114−6127.
(37) Atkinson, D. B.; Hudgens, J. W. *J. Phys. Chem. A* **1999**, *103*, 4242−4252.
(38) King, K. D. *Int. J. Chem. Kinet.* **1979**, *11*, 1071−1080.

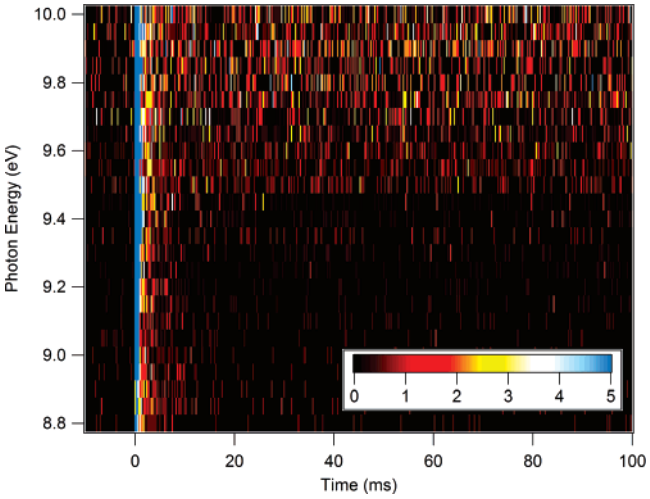

Figure 7. Time- and photon-energy-resolved measurements of $C_3H_3^+$ (m/z = 39) photoionization signal following photolysis of propargyl bromide in the presence of O_2.

with $\Delta_f H^\circ_0(CH_2{=}C{=}CHOO)$ allows calculation of the enthalpy of formation of $CH_2{=}C{=}CHOO^+$ via the simple equation

$$\Delta_f H^\circ_0(CH_2{=}C{=}CHOO^+) = \Delta_f H^\circ_0(CH_2{=}C{=}CHOO) + \mathrm{AIE}(CH_2{=}C{=}CHOO) \quad (3)$$

The value (1162 ± 8) kJ mol^{-1} compares very well with the CBS-QB3 $\Delta_f H^\circ_0(CH_2{=}C{=}CHOO^+)$ of 1164 kJ mol^{-1}, evaluated using eq 4 and the computed adiabatic ionization energy and enthalpy of formation. From $\Delta_f H^\circ_0(CH_2{=}C{=}CHOO^+)$ and $\Delta_f H^\circ_0(C_3H_3^+)$ it is also possible to extract the bond energy $D^\circ_0([CH_2{=}C{=}CH]^+{-}OO)$ of 19 kJ mol^{-1} (0.20 eV) using

$$D^\circ_0([CH_2{=}C{=}CH]^+{-}OO) = \Delta_f H^\circ_0(C_3H_3^+) - \Delta_f H^\circ_0(CH_2{=}C{=}CHOO^+) \quad (4)$$

The spin multiplicity of the cations of 1-alkenylperoxy radicals can be rationalized by relatively simple MO considerations. As pointed out by Meloni et al.[5] hyperconjugation reduces the stability of alkylperoxy cations, making the cation ground state weakly bound or unbound with respect to the ground state (alkyl cation + O_2) fragments. Among the alkylperoxy radicals investigated, only methylperoxy has a bound cation ground state. From computational and experimental results the ground states of alkylperoxy cations are triplets, implying that the photoionization occurs by removal of an electron from the doubly occupied bonding σ_{C-O} MO instead of detachment of the unpaired electron mainly localized on the terminal oxygen. The explanation is that the removal of the electron from the bonding σ_{C-O} allows the system to lower its total energy by further stabilization of the fragment (R^+) via hyperconjugation. This is ultimately the reason why alkylperoxy radicals larger than methylperoxy have unbound cations. In the case of 1-alkenylperoxy, the major difference with respect to alkylperoxy is that the HOMO is antibonding. Therefore, the removal of the electron from the antibonding HOMO stabilizes the molecule in such a way that the resulting cation is bound. We can generalize this behavior with a rule.

Alkylic peroxy radicals dissociatively ionize, with the exception of methylperoxy, whereas 1-alkenylperoxy radicals have stable singlet ground electronic state cations. This rule is simply explained in terms of fragment stabilization effects (hyperconjugation) for the alkyl-type peroxy, while for alkenylic-type peroxy radicals the formation of stable cations is due to the antibonding character of the neutral HOMO.

A further validation of this molecular orbital picture is given by the experimental appearance energy (AE) of propargyl caused by the dissociative ionization of the less stable "alkylic-type" propargylperoxy, $OOCH_2{-}C{\equiv}CH$. Also in this case, the cation is not bound because the ionization proceeds via electron detachment from the neutral HOMO−1, which is a bonding σ_{C-O} MO, followed by resonance stabilization of the propargyl cation. Figure 7 shows a two-dimensional image of the time- and photon-energy dependent propargyl signal from photodissociation of propargyl bromide in the presence of 4.7×10^{16} molecule cm^{-3} O_2. As a function of time, the signal rapidly returns to baseline for energies below 9.5 eV. At higher photon energies $C_3H_3^+$ persists to longer times. This signal is likely due to dissociative ionization of $OOCH_2{-}C{\equiv}CH$. The approximate appearance energy of 9.5 eV is in good agreement with the calculated AIE($OOCH_2{-}C{\equiv}CH$) of 9.47 eV.

Conclusions

Multiplexed time-resolved photoionization mass spectrometry has been employed to investigate the ionization behavior of two 1-alkenyl peroxy radicals. From the photoionization efficiency curves and Franck−Condon simulation the first experimental values for the adiabatic ionization energies of 1-*c*-C_5H_7OO and $CH_2{=}C{=}CHOO$ have been determined as (8.70 ± 0.05) eV and (9.32 ± 0.05) eV, respectively. From the fitted FC spectral simulation, the splitting between the singlet and triplet cation electronic states is derived as (0.76 ± 0.05) eV and (0.80 ± 0.15) eV for 1-*c*-C_5H_7OO and $CH_2{=}C{=}CHOO$, respectively. For the 1-propadienylperoxy (propargylperoxy) radical, the AIE together with the heat of formation provide the $\Delta_f H^\circ_0(CH_2{=}C{=}CHOO^+)$ of 1162 ± 8 kJ mol^{-1} that compares very well with the CBS-QB3 value. From $\Delta_f H^\circ_0(CH_2{=}C{=}CHOO^+)$ and $\Delta_f H^\circ_0(C_3H_3^+)$ it is also possible to extract the bond energy $D^\circ_0(CH_2{=}C{=}CH^+{-}OO)$ of 19 kJ mol^{-1} (0.20 eV). In addition, using a molecular orbital argument, we generalize the ionization behavior of alkylperoxy and 1-alkenylperoxy radicals with a rule, which states that the alkylperoxy radicals dissociatively ionize due to stabilization effects of the fragments, whereas the 1-alkenylperoxy radicals have stable singlet ground state cations because the ionization occurs by electron removal from the antibonding HOMO.

Acknowledgment. We thank Mr. Howard Johnsen for excellent technical support. This work is supported by the Division of Chemical Sciences, Geosciences, and Biosciences, the Office of Basic Energy Sciences, the U.S. Department of Energy. Sandia is a multiprogram laboratory operated by Sandia Corporation, a Lockheed Martin Company, for the National Nuclear Security Administration under Contract DE-AC04-94-AL85000. The Advanced Light Source is supported by the Director, Office of Science, Office of Basic Energy Sciences, Materials Sciences Division, of the U.S. Department of Energy under Contract No. DE-AC02-05CH11231 at Lawrence Berkeley National Laboratory.

Supporting Information Available: Complete ref 23. This material is available free of charge via the Internet at http://pubs.acs.org.

JA075130N